Space-time nonseparable pulses: Constructing isodiffracting donut pulses from plane waves and single-cycle pulses

Apostolos Zdagkas,[1,*] Nikitas Papasimakis,[1] Vassili Savinov,[1] and Nikolay I. Zheludev[1,2]
[1]*Optoelectronics Research Centre and Centre for Photonic Metamaterials, University of Southampton, Southampton SO17 1BJ, United Kingdom*
[2]*Centre for Disruptive Photonic Technologies, School of Physical and Mathematical Sciences and The Photonics Institute, Nanyang Technological University, Singapore 637378, Singapore*

(Received 20 August 2020; accepted 6 November 2020; published 8 December 2020)

Maxwell's equations can be satisfied not only by plane electromagnetic waves, but also by more exotic space-time nonseparable electromagnetic pulses which cannot be represented as a product of time- and space-dependent functions. A family of such pulses with finite energy was identified by Ziolkowski [Phys. Rev. A **39**, 2005 (1989)]. Later, Hellwarth and Nouchi [Phys. Rev. E **54**, 889 (1996)] highlighted a subset of Ziolkowski's pulses, now known as flying donuts, a formation of polarization singularities of toroidal topology traveling at the speed of light. Spurred by recent advances in ultrafast and topological optics, space-time nonseparable electromagnetic excitations are now becoming the focus of growing experimental efforts as they hold promise for topological information transfer, probing and inducing transient excitations in matter such as anapole and toroidal modes. Here we demonstrate that the flying donut can be constructed from an ensemble of monochromatic plane waves with continuous spatial and frequency spectrum and hence can be generated by converting broadband conventional transverse electromagnetic pulses.

DOI: 10.1103/PhysRevA.102.063512

I. INTRODUCTION

Flying donuts (FDs) are single-cycle pulses with toroidal electromagnetic field configuration and unusual spatiotemporal coupling [1]. FD pulses exhibit a fine topological structure along with regions where energy back-propagation occurs [2], while their interaction with simple homogeneous media is nontrivial [3]. They form the free-space propagating counterparts of toroidal excitations in matter, i.e., charge-current configurations with donutlike topology [4,5]. In fact, it has been shown that flying donut pulses can efficiently engage dynamic toroidal and anapole excitations in dielectric particles, even when the latter does not possess toroidal symmetry [3,6].

Flying donuts were introduced in the context of Brittingham's work on "focus wave modes" where he described a new class of wide-band nondiffracting pulses, localized solutions to Maxwell's equations [7]. Soon after, Ziolkowski showed that, although "focus wave modes" are unphysical and have infinite energy [8], a finite-energy pulse can be constructed from superposition of such modes [9]. In fact, these finite-energy pulses originate from modified Gaussian pulses that emerge as solutions of the scalar wave equation with moving complex sources. An example of such a pulse is the "splash pulse" [10]. In 1996 Hellwarth and Nouchi found special cases of Ziolkowski's solution, space-time nonseparable finite-energy linearly polarized "pancake pulses [11,12] and flying donut pulses of toroidal symmetry [1].

Although the generation of electromagnetic and acoustic analogs of localized pulses based on Ziolkowski's solutions has been presented in the literature [13–15], the generation of electromagnetic FDs only recently been demonstrated [16,17]. The generation of FD pulses requires to address simultaneously their few cycle nature, toroidal symmetry, and importantly space-time coupling (STC) that manifests as a frequency dependent transverse profile. Although apparent in the time domain, STCs can sometimes be more intuitively studied in the frequency domain as space-spectrum couplings. Evidently, a plane-wave expansion is highly desirable for the generation and study of light-matter interactions of FD pulses.

In this work, we provide closed-form expressions for the time-frequency Fourier transform of the pulse. We use the derived analytical expressions to highlight the space-spectrum couplings in the FD pulse. In fact, we show that in the paraxial regime the pulse exhibits isodiffracting propagation, i.e., in each cross section of the beam perpendicular to the direction of propagation the spatial profiles of intensity for every frequency component scale in the same way along the trajectory of the beam. We expect that this type of propagation invariance will be useful for energy transfer applications like free-space communications and micromachining. The frequency domain expressions reported here facilitate the generation and characterization of FDs [16,17], as well as the study of their interactions with matter through efficient Fourier propagation methods [18]. In addition, we present a simple expression for the spatial Hankel transform that reveals the focusing properties of FDs and leads to a semianalytical plane-wave expansion of the pulse. The latter is used

*a.zdagkas@soton.ac.uk

 ©2020 American Physical Society

to reveal hidden features of the pulse, such as the role of back-propagating plane waves in the nonparaxial regime and it provides an insight on how the simplest form of linear polarized electromagnetic waves can be combined to generate a pulse with complex spatiotemporal and vectorial structure.

II. TIME-FREQUENCY FOURIER TRANSFORM OF THE FLYING DONUT

The flying donut pulse can exist in transverse electric (TE) and transverse magnetic (TM) field configurations. In the TE case, the electric field is azimuthally polarized, whereas the magnetic is longitudinally and radially oriented. The TM pulse can be derived from the TE by exchanging the electric and magnetic fields as follows:

$$\mathbf{E}_{\mathrm{TM}} = \sqrt{\frac{\mu_0}{\epsilon_0}}\mathbf{H}_{\mathrm{TE}}, \tag{1}$$

$$\mathbf{H}_{\mathrm{TM}} = -\sqrt{\frac{\epsilon_0}{\mu_0}}\mathbf{E}_{\mathrm{TE}}, \tag{2}$$

and describes a radially polarized FD.

The FD pulse itself emerges from a scalar "seed function" [1]

$$f(t,\ \mathbf{r}) = f(t,\ \rho, z) = \frac{1}{\rho^2 - [(ct - z) + iq_1][(ct + z) + iq_2]} \tag{3}$$

which is a solution of the scalar wave equation. Here, ρ and z are the radial and longitudinal coordinates, t is the time, c is the speed of light in vacuum, while q_1 and q_2 are free parameters that, as will become apparent later in the text, define the central frequency and the focusing strength of the pulse, respectively. In a cylindrical coordinate system the electric (**E**) and magnetic (**B**) fields of the TE FD pulse are derived from the following equations [1,19]:

$$E_\theta = \mu_0 \partial_t \partial_\rho f,$$
$$B_\rho = \mu_0 \partial_z \partial_\rho f,$$
$$B_z = \mu_0 \left(\partial_z^2 f - \frac{1}{c^2}\partial_t^2 f \right),$$

where ∂_t, ∂_ρ, ∂_z are the partial derivatives with respect to t, ρ, and z.

The azimuthally polarized TE FD pulse can therefore be presented as [11]

$$E_\theta = -4if_0\sqrt{\frac{\mu_0}{\epsilon_0}}\frac{\rho(q_1 + q_2 - 2ict)}{[\rho^2 + (q_1 + i\tau)(q_2 - i\sigma)]^3}, \tag{4}$$

$$H_\rho = 4if_0\frac{\rho(q_2 - q_1 - 2iz)}{[\rho^2 + (q_1 + i\tau)(q_2 - i\sigma)]^3}, \tag{5}$$

$$H_z = -4f_0\frac{\rho^2 - (q_1 + i\tau)(q_2 - i\sigma)}{[\rho^2 + (q_1 + i\tau)(q_2 - i\sigma)]^3}, \tag{6}$$

where ϵ_0 and μ_0 are the vacuum permittivity and permeability, respectively, $\tau = z - ct$, $\sigma = z + ct$, and f_0 a constant defining the amplitude and the units. The pulse is defined by q_1 and q_2 and from now on we assume that $q_1 \leqslant q_2$. When compared to a Gaussian beam, q_1 has the role of the wavelength and q_2 the role of the Rayleigh length. Similarly to Gaussian pulses, FD pulses can be focused. Both real and imaginary parts are solutions to Maxwell's equations, termed here "1-cycle" and"$1\frac{1}{2}$-cycle," respectively, reflecting their duration at focus [see Figs. 1, 2(a) and 2(b)]. Owing to Gouy phase shifts, the shape of the pulse at focus is different from that in the far field [11] with the real (imaginary) part transforming from "$1\frac{1}{2}$-cycle" ("1-cycle") away from focus to a "1-cycle" pulse ("$1\frac{1}{2}$-cycle") at focus (see Fig. 1).

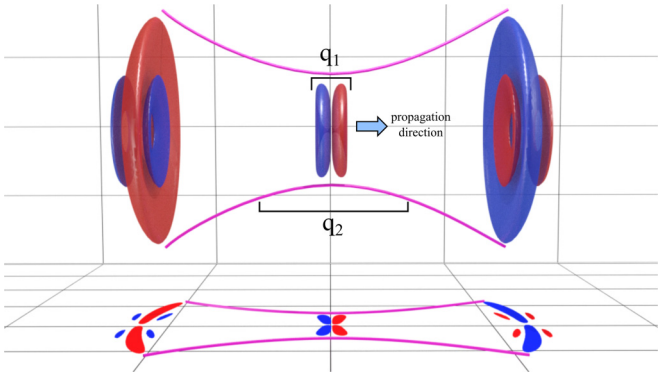

FIG. 1. Propagation of the single-cycle TE FD pulse. Owing to the Gouy phase shift, a "$1\frac{1}{2}$-cycle" pulse (left) transforms into a "1-cycle" pulse at focus (center), and resumes its "$1\frac{1}{2}$-cycle" duration after propagating through the focal region (right). The fact that the pulse acquires a π phase by traveling through the focus is also shown from the phase reversal of the electric field, depicted by blue and red colors.

To date, exact closed-form expressions for the FD pulse have only been defined in the time domain. Although the time domain expressions (4)–(6) allow to describe the FD pulse in a compact fashion, frequency domain expressions are crucial for generating and understanding the propagation dynamics of FDs. We have derived analytically such

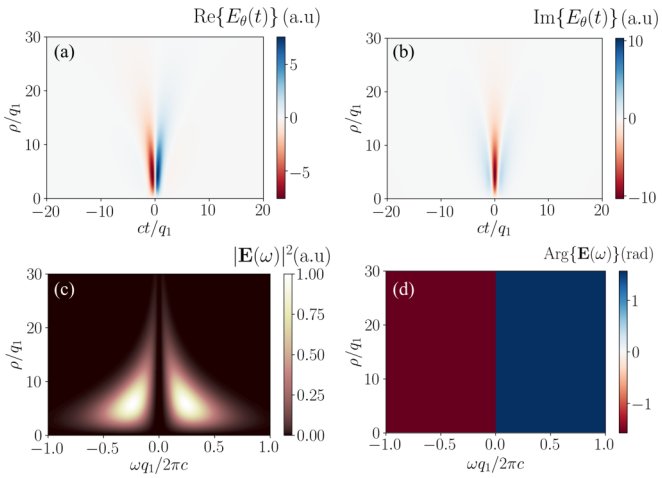

FIG. 2. (a), (b) Time-radius cross sections of the electric field of the "1-cycle" and "$1\frac{1}{2}$-cycle" TE pulses, respectively, at their focus for $q_2 = 100q_1$. (c), (d) Radial distribution of spectral power (c) and spectral phase (d) of the TE "1-cycle" pulse. The spectral phase is $-\pi/2$ for negative and $\pi/2$ for positive frequencies.

expressions for both the real and imaginary parts of the TE and TM pulses (see Appendix A). Here, we focus on the real part of the TE FD pulse (the "1-cycle" azimuthally polarized pulse):

$$E_{\mathrm{re}}(\omega)=\begin{cases}4f_0\sqrt{\mu_0/\epsilon_0}\Big[i\pi\frac{\omega}{c^2}\frac{\rho}{q_1}e^{-\frac{\omega(q_2+q_1)}{2c}}\frac{e^{\frac{i\omega}{2c}\sqrt{A}}(2ci+\omega\sqrt{A})+e^{-\frac{i\omega}{2c}\sqrt{A}}(-2ci+\omega\sqrt{A})}{2A^{3/2}}\Big]^*, & \omega>0\\ 4f_0\sqrt{\mu_0/\epsilon_0}i\pi\frac{\omega}{c^2}\frac{\rho}{q_1}e^{\frac{\omega(q_2+q_1)}{2c}}\frac{e^{-\frac{\omega i}{2c}\sqrt{A}}(-2ci+\omega\sqrt{A})+e^{\frac{\omega i}{2c}\sqrt{A}}(2ci+\omega\sqrt{A})}{2A^{3/2}}, & \omega<0\\ 0, & \omega=0\end{cases} \tag{7}$$

with

$$A\equiv A(\rho,z,q_2)=-(-q_1+q_2-2\rho-2iz)\times(-q_1+q_2+2\rho-2iz). \tag{8}$$

Equation (7) allows us to examine the spectral phase of the FD pulse. From Eq. (8) one can see that at focus $\sqrt{A}$ is either real $\rho\geqslant(q_2-q_1)/2$, or imaginary $\rho<(q_2-q_1)/2$, and in both cases it leads to an imaginary field in the frequency domain for any radius. Since the field has flat spectral phase $\theta(\rho,\omega)=\pm\pi/2$ [see Fig. 2(d)], the pulse described by Eqs. (4)–(6) is bandwidth limited. Away from the focus, the spectral phase has terms exponential on $\omega\sqrt{A}$, and since A is a quadratic function of ρ, these terms are nonseparable functions of frequency ω and coordinate ρ.

In Fig. 2(c), we plot the radial distribution of spectral power of the pulse at focus, $z=0$, where the space-frequency coupling becomes apparent. The spectrum is broad at the central part of the pulse and narrows towards the peripheral parts, where lower-frequency components are prominent. FDs belong to the class of isodiffracting pulses in which the intensity transverse spatial profiles scale along the trajectory of the pulse in the same way for all frequency components. The isodiffracting nature of FD becomes clear in Fig. 3 where the FD and a nonisodiffracting pulse composed of Hermite-Gauss beams are compared. A false color image made of all the composing frequencies of the pulse and a plot with the trace of the position of the maximum intensity for each frequency are plotted. The isodiffracting nature of the FD leads to a separation of the wavelengths with the maxima of the longer wavelengths located at larger radii and the shorter wavelengths closer to the center at any propagation distance, as it is also shown in Fig. 2(c). In contrast, in the nonisodiffracting Hermite-Gauss pulse the maxima of the longer wavelengths are strongly focused resulting in different lateral spectral profiles for different propagation distances. The isodiffracting nature of the FD pulse can be rigorously derived in the case of well-collimated pulses ($q_2\gg q_1$) (see Appendix B).

III. SPATIAL HANKEL TRANSFORM OF THE FLYING DONUT

Owing to its toroidal field configuration, the FD pulse is rotationally symmetric and thus can be expanded in cylindrically symmetric single-cycle pulses by virtue of the Hankel transform [18]. The Hankel transform of the electric field for the TE pulse can be derived as (see Appendix C)

$$\mathbf{E}_\theta(k_\rho)=-\pi f_0\sqrt{\frac{\mu_0}{\epsilon_0}}(q_1+q_2-2ict)\frac{k_\rho^2}{\alpha}K_1(k_\rho\alpha)\hat{\boldsymbol{\theta}}, \tag{9}$$

with $\alpha=\sqrt{(q_1+iz-ict)(q_2-iz-ict)}$ and K_1 the first-order modified Bessel function of the second kind. The transforms of the real and imaginary parts, or the 1-cycle and $1\frac{1}{2}$-cycle, are given by

$$E_{\mathrm{re},\theta}(k_\rho)=\frac{E_\theta(k_\rho)-E_\theta^*(k_\rho)}{2}, \tag{10}$$

$$E_{\mathrm{im},\theta}(k_\rho)=\frac{E_\theta(k_\rho)+E_\theta^*(k_\rho)}{2i}, \tag{11}$$

respectively.

The closed-form expression is a well-behaved function in contrast to the numerical Hankel transform that is inaccurate close to the axis of symmetry [20]. It also simplifies the study of the pulse in momentum space which provides information

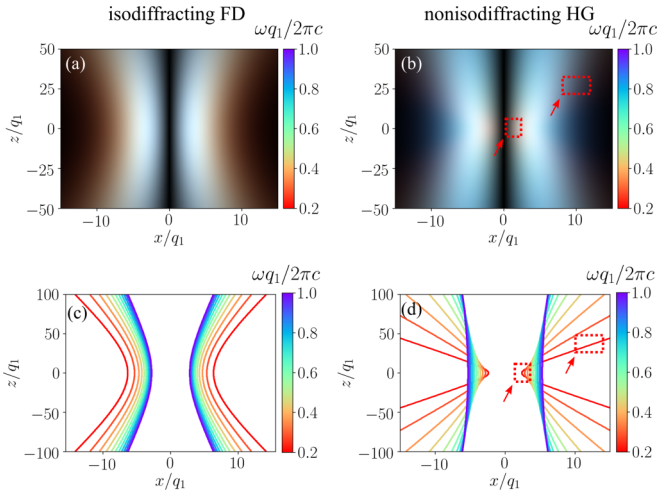

FIG. 3. (a), (b) False color representation of x-z cross sections at $y/q_1=0$ of the electric field intensity of the spectral components of the isodiffracting FD pulse and of a nonisodiffracting Hermite-Gauss beam, respectively. The range of presented frequency components spans the full bandwidth of the FD pulse. The brightness represents the intensity distribution in space while color corresponds to the different wavelengths. Blue and red colors present shorter and longer wavelengths, respectively. (c), (d) Traces of the position of the maximum intensity for each wavelength for the FD (c) and a nonisodiffracting Hermite-Gauss beam (d). In the case of the FD pulse the intensity maxima of different wavelength components do not mix upon propagation with high frequencies (blue lines) dominating at the center of the pulse and the lower frequencies (red lines) at the periphery. For the nonisodiffracting Hermite-Gauss beam the spectral components mix at focus with the lower frequencies being tightly focused and hence later being strongly diffracted [see areas highlighted by the red squares in (b) and (d)].

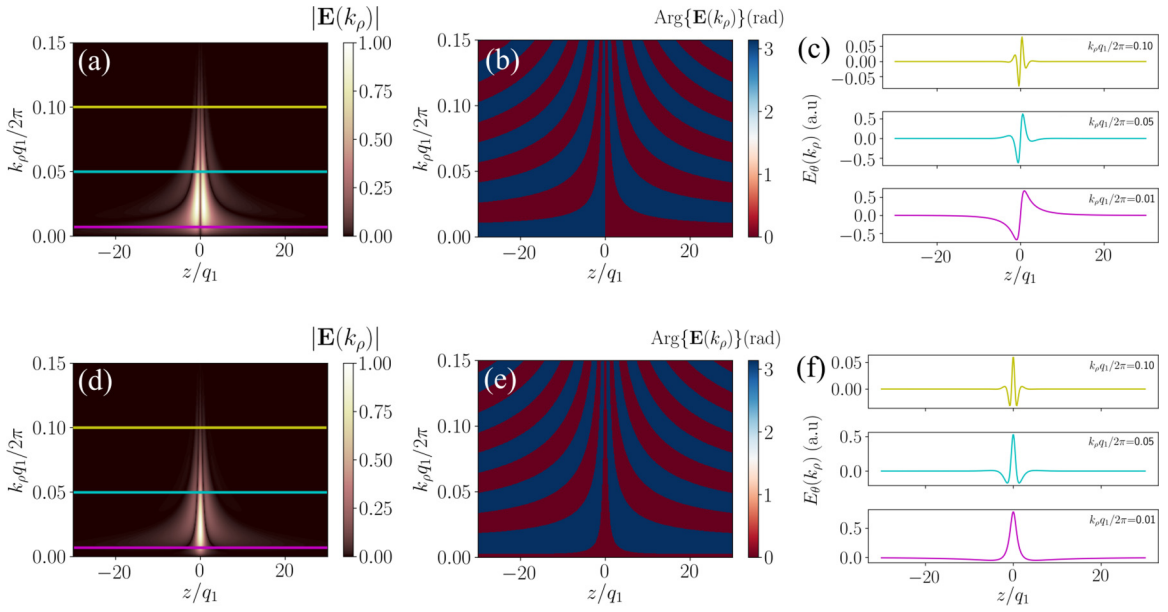

FIG. 4. Amplitude and phase of the Hankel transforms of the "1-cycle" (a), (b), and "$1\frac{1}{2}$-cycle" (d), (e), electric fields at focus, $t = 0$, and for $q_2 = 100q_1$. The phase at (b) and (c) alternates between 0 and π. (c), (f) The imaginary part of the Hankel transform of the "1-cycle" and "$1\frac{1}{2}$-cycle" pulses at three different values of k_ρ as indicated by the horizontal lines in (a) and (d).

about its focusing properties. Figure 4 shows the electric field Hankel transforms of the 1-cycle [Figs. 4(a) and 4(b)], and $1\frac{1}{2}$-cycle [Figs. 4(d) and 4(e)] pulses at focus ($t = 0$) for $q_2 = 100q_1$. The former is antisymmetric with respect to the z coordinate and vanishes at $z = 0$ and $t = 0$ [see Fig. 4(c)]. On the other hand, the Hankel transform of the $1\frac{1}{2}$-cycle pulse is symmetric with respect to z and peaks at $z = 0$.

The Hankel transform decomposes the FD pulse into a set of pulses with different focusing strengths. As a result, Figs. 4(c) and 4(f) illustrate that the FD is composed out of weakly focused (low-k_ρ) single-cycle pulses (magenta colored line) and strongly focused (high-k_ρ) blueshifted broader pulses (yellow line). It exhibits a flat radial spectral phase profile at $z = 0$ [Figs. 4(b) and 4(e)] indicating that at focus the FD pulse can be decomposed in a set of in-phase cylindrically symmetric pulses. Away from focus the sign of the phase alternates with increasing spatial frequency, a trait which is related to the isodiffracting nature and fine topological structure of the pulse [2].

IV. PLANE-WAVE EXPANSION OF THE FLYING DONUT PULSE

The Hankel transform allows to readily expand the FD pulse into plane waves. Indeed, for the plane-wave expansion of the FD pulse, two spatial $[(\rho, z) \to (k_\rho, k_z)]$ and one temporal $[t \to \omega]$ transform is required, of which only one at a time can be derived analytically (either time-frequency Fourier or Hankel transform). Since the radial transform is given by a simple analytical expression, the Fourier transform of the two remaining dimensions, time and longitudinal position, can be easily performed numerically. The result of the plane-wave decomposition is presented in Fig. 5 for three different cases: $q_2 = 2q_1$, $q_2 = 10q_1$, and $q_2 = 100q_1$. The decomposition is given at the surface of a cone that represents the cone of light (defined by $\omega = c|k|$). Only positive k_ρ are presented since the pulse is azimuthally symmetric. The first row depicts the projection of that cone in the k_ρ-k_z plane, the third row depicts the projection in the frequency-radial spatial frequency ν-k_ρ plane, while in the middle row a three-dimensional (3D) view of the plane-wave expansion is presented. The colors represent the squared amplitude of the plane-wave components. The plot is given only for positive frequencies.

Figure 5(a) indicates that in the extreme nonparaxial regime, where $q_2 \simeq q_1$, backward propagating waves are present in the FD pulse. This is revealed by the appearance of negative k_z for positive frequencies. However, by increasing q_2 with respect to q_1, we notice that the contribution of backward propagating waves rapidly vanishes. Moreover, we observe a decrease of k_ρ in favor of k_z, indicating that the pulse is weakly focused and hence it propagates as a paraxial pulse ($q_2 \gg q_1$). The existence of forward and backward propagating waves emanates from Eq. (3) as discussed in Refs. [9,21]. The space-time nonseparability reveals itself in the $\mathbf{k}$-ω domain, where low (high) frequencies correspond to small (large) range of radial wave vectors indicating that they are weakly (strongly) confined in the transverse plane. In addition, we note that small (large) radial wave vectors k_ρ are accompanied by a narrower (broader) bandwidth, as is evident in Fig. 5(h). This behavior is in accordance with the isodiffracting nature of the FD pulse (see also discussion in Sec. II).

The presented decomposition of the pulse into plane waves illustrates how the simplest form of electromagnetic waves with linear polarization can be combined to generate a pulse with complex spatiotemporal and vectorial structure. Previous analysis of localized waves, in particular "focus wave modes," has highlighted the importance of considering the description and generation of space-time coupled pulses in the frequency

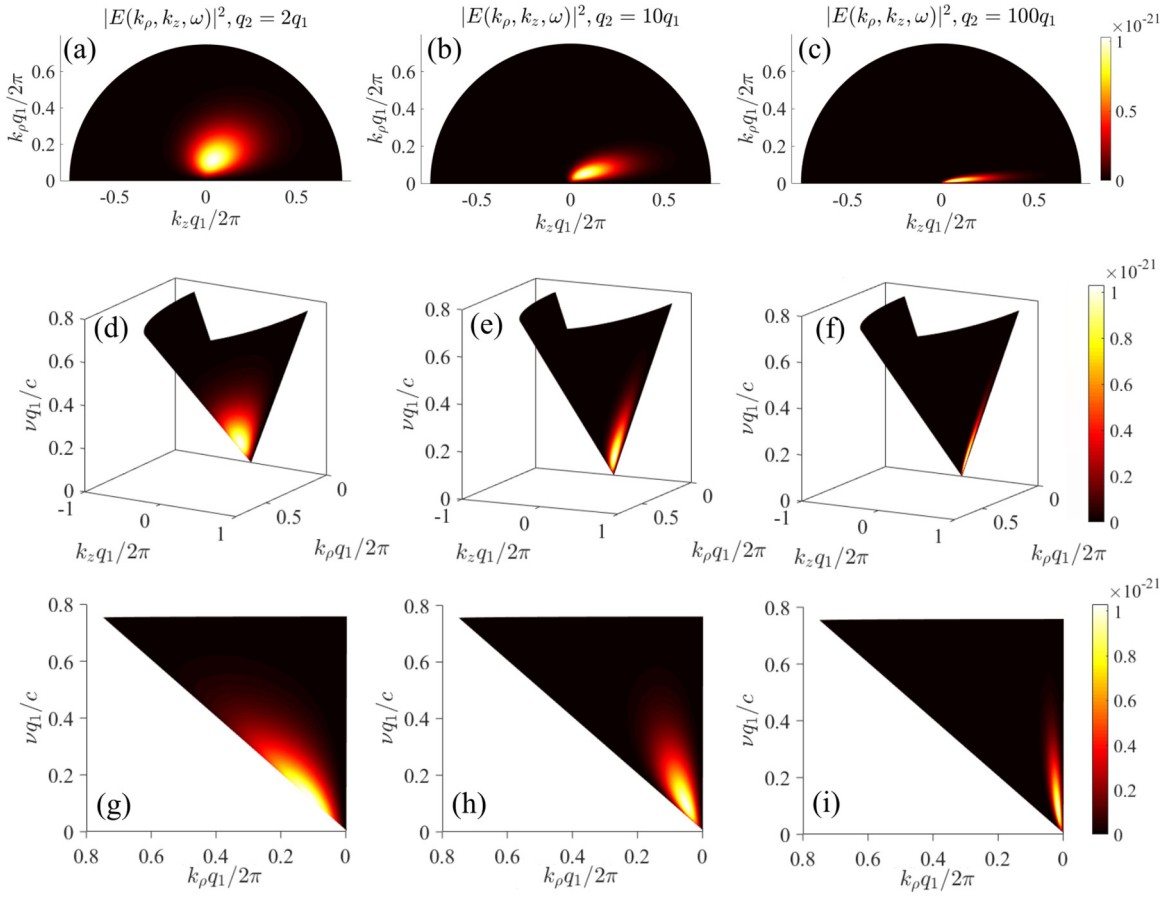

FIG. 5. Plane-wave decomposition of the FD pulse presented on the surface of a half-cone, representing the cone of light ($\omega = ck$). (a)–(c) The k_ρ-k_z projection of the decomposition. (d)–(f) Full three-dimensional presentation of the plane-wave spectrum on the light cone. (g)–(i) The ν-k_ρ projection of the decomposition. The colors represent the squared electric field amplitude of the plane waves in arbitrary units. Only positive frequencies are considered.

domain [22,23]. In these works, plane waves whose amplitude is described by a nonseparable equation in $\mathbf{k}$-ω space can be combined to form space-time coupled solutions of the scalar wave equation. A weighted superposition of such waves also results in a space-time coupled solution. In a similar manner, the plane-wave expansion of the FD provides an invaluable tool for the study of its propagation dynamics and light-matter interactions and will inform the development and implementation of generation and detection schemes for FD pulses.

V. SUMMARY

In this paper we have presented a series of decompositions of the FD pulse. We have derived closed-form expressions for the Fourier transform and provided a frequency domain description of the FD pulse. The Fourier transform expression indicates that the FD pulse is space-spectrum nonseparable and in fact very close to an ideal isodiffracting pulse, a property that ensures the preservation of its spectral profile upon propagation. In addition, the Fourier decomposition of the pulse into monochromatic beams facilitates the study of its propagation properties by enabling the use of efficient frequency domain propagation techniques [18]. Moreover, such a decomposition can be used not only for the study of the pulse propagation dynamics, but also for the description of the interaction of the FD pulse with matter. The Hankel transform derived here allows to describe the radial spectrum in momentum space and hence reveals information related to the focusing properties of the pulse. It can provide an accurate picture of the spatial frequency distribution of the pulse and hence allows for the decomposition of FDs into plane waves. The plane-wave expansion reveals the properties of the complex FD pulse by breaking it down to simple linearly polarized waves. It provides a complementary representation to the time domain one and can reveal properties, such as the degree of focusing of the FD pulse and the existence of backward propagating waves in the strongly nonparaxial regime.

The spatiotemporal description of FDs in different representations provides a framework for the generation, detection, and study of light-matter interactions of such complex pulses. Pulses whose spatiospectral profile does not change upon propagation could be important in all applications involving pulsed energy transfer, such as free-space telecommunications, spectroscopy, and manufacturing by light.

The data from this paper can be obtained from the University of Southampton ePrints research repository [24].

ACKNOWLEDGMENTS

The authors acknowledge the support of the MOE Singapore (Grant No. MOE2016-T3-1-006), the UK Engineering and Physical Sciences Research Council (Grant No. EP/M009122/1), the European Research Council (Advanced Grant No. FLEET-786851), and the Defense Advanced Research Projects Agency (DARPA) under the Nascent Light Matter Interactions program. We thank the anonymous reviewer for indicating an alternative route to calculate the Hankel transform of Appendix C.

APPENDIX A: FOURIER TRANSFORM

In this Appendix a step-by-step derivation of an analytical expression for the time-frequency Fourier transform of the FD pulse is presented. The following Fourier transform pair is used:

$$\mathbf{F}(\mathbf{r},\omega)=\int_{-\infty}^{\infty}e^{i\omega t}\mathbf{F}(\mathbf{r},t)dt, \tag{A1}$$

$$\mathbf{F}(\mathbf{r},t)=\frac{1}{2\pi}\int_{-\infty}^{\infty}e^{-i\omega t}\mathbf{F}(\mathbf{r},\omega)d\omega. \tag{A2}$$

For the transverse electric field (TE) we have [1]

$$E_\theta=-4if_0\sqrt{\frac{\mu_0}{\epsilon_0}}\frac{\rho(q_1+q_2-2ict)}{[\rho^2+(q_1+i\tau)(q_2-i\sigma)]^3}, \tag{A3}$$

$$H_\rho=4if_0\frac{\rho(q_2-q_1-2iz)}{[\rho^2+(q_1+i\tau)(q_2-i\sigma)]^3}, \tag{A4}$$

$$H_z=-4f_0\frac{\rho^2-(q_1+i\tau)(q_2-i\sigma)}{[\rho^2+(q_1+i\tau)(q_2-i\sigma)]^3}, \tag{A5}$$

with $\tau=z-ct$ and $\sigma=z+ct$. For convenience and generality, we will use dimensionless variables. More specifically, we write everything with respect to q_1 which has dimensions of length. As such, we define $\rho'=\rho/q_1$, $z'=z/q_1$, $q_2'=q_2/q_1$, $t'=ct/q_1$, and $\omega'=q_1\omega/c$ and we omit the coefficients $4f_0\sqrt{\mu_0/\epsilon_0}/q_1^4$ and $4f_0/q_1^4$ for the electric and the magnetic fields, respectively. Finally, we omit the primes on the new dimensionless variables for clarity. Now, the dimensionless fields are given by the following equations:

$$E_\theta=-i\frac{\rho(1+q_2-2it)}{[\rho^2+(1+iz-it)(q_2-iz-it)]^3}, \tag{A6}$$

$$H_\rho=i\frac{\rho(q_2-1-2iz)}{[\rho^2+(1+iz-it)(q_2-iz-it)]^3}, \tag{A7}$$

$$H_z=-\frac{\rho^2-(1+iz-it)(q_2-iz-it)}{[\rho^2+(1+iz-it)(q_2-iz-it)]^3}. \tag{A8}$$

We will first work with the electric field. From now on and for clarity we will refer to the electric field as E, but we actually mean that we are using the θ component. The real and imaginary parts of the field are quite complex expressions to compute the Fourier integral. Thus, and because of the linearity of the integral operator, we will calculate the Fourier transform of the complex field and then we will take the real and imaginary parts from the equations

$$E_{\mathrm{re}}(\omega)=\frac{E(\omega)+E^*(-\omega)}{2} \tag{A9}$$

and

$$E_{\mathrm{im}}(\omega)=\frac{E(\omega)-E^*(-\omega)}{2i}. \tag{A10}$$

Proof.

$$\begin{aligned}E_{\mathrm{re}}(\omega)&=\int_{-\infty}^{+\infty}e^{i\omega t}\mathrm{Re}[E(t)]dt\\&=\int_{-\infty}^{+\infty}\frac{e^{i\omega t}E(t)+[e^{-i\omega t}E(t)]^*}{2}dt\\&=\frac{E(\omega)+E^*(-\omega)}{2}.\end{aligned}$$

■

These correspond to the 1-cycle and $1\frac{1}{2}$-cycle,respectively.

Returning now to Eq. (A6), it is apparent that we can apply Jordan's lemma since the power of t on the denominator is five times bigger than that of the numerator. Thus, the Fourier transform is given by the integral residues on the upper and lower half-complex-plane [25]. One only has to find the poles and determine when they are located in upper half or lower half-plane.

From (A6), it is apparent that the equation has two triple poles, thus only two distinct. Luckily, they are both located in the lower half-plane, though the algebra to prove this is elaborate. We are going to prove this explicitly, though an alternative proof was presented on [12].

We start by writing the poles

$$t_1=\tfrac{1}{2}(\sqrt{-(-1+q_2-2\rho-2iz)(-1+q_2+2\rho-2iz)}-iq_2-i), \tag{A11}$$

$$t_2=\tfrac{1}{2}(-\sqrt{-(-1+q_2-2\rho-2iz)(-1+q_2+2\rho-2iz)}-iq_2-i). \tag{A12}$$

It is useful here to define

$$\begin{aligned}A\equiv A(\rho,z,q_2)&=-(-1+q_2-2\rho-2iz)(-1+q_2+2\rho-2iz)\\&=4z^2+4\rho^2-(q_2-1)^2+4(q_2-1)iz.\end{aligned} \tag{A13}$$

Now we want to prove that

$$\mathrm{Im}\begin{pmatrix} t_1 \\ t_2 \end{pmatrix} = \frac{1}{2}\left\{ -1-q_2 \pm \{(4z-4zq_2)^2 + [4\rho^2+4z^2-(q_2-1)^2]^2\}^{1/4} \sin\left[\frac{1}{2}\mathrm{Arg}(A)\right]\right\} \tag{A14}$$

is negative for every $q_2 \geqslant 1$, $\rho \geqslant 0$, and z. We will prove it for t_1.

Proof.

$$\mathrm{Arg}(x+iy) = \mathrm{atan2}(y,x) = \begin{cases} \arctan\left(\frac{y}{x}\right), & x>0 \\ \arctan\left(\frac{y}{x}\right)+\pi, & x<0 \text{ and } y \geqslant 0 \\ \arctan\left(\frac{y}{x}\right)-\pi, & x<0 \text{ and } y<0 \\ +\frac{\pi}{2}, & x=0 \text{ and } y>0 \\ -\frac{\pi}{2}, & x=0 \text{ and } y<0 \\ \text{undefined}, & x=0 \text{ and } y=0. \end{cases} \tag{A15}$$

(i) For $q_2 = 1$ or $z = 0$, it is immediately apparent from (A11) that $\mathrm{Im}(t_1) < 0$.

(ii) For $z < 0$, $\mathrm{Arg}(A) < 0$ and thus $\mathrm{Im}(t_1) < 0$.

(iii) For $z > 0$, we make use of the trigonometric identity $\sin[\arctan(x)] = \frac{x}{1+x^2}$ and some other more common identities. It can be shown that all the remaining cases

(a) $4z^2+4\rho^2-(q_2-1)^2 > 0$,

(b) $4z^2+4\rho^2-(q_2-1)^2 < 0$,

(c) $4z^2+4\rho^2-(q_2-1)^2 = 0$ give $\mathrm{Im}(t_1) < 0$. ■

A similar analysis holds for the second pole as well. Knowing that the poles are located in the lower half complex plane, the integral can be calculated from the integral residues

$$\int_{-\infty}^{+\infty} e^{i\omega t}E(t)dt = 2\pi i \sum_i \mathrm{Res}[e^{i\omega t}E(t), t_i]I, \tag{A16}$$

with I denoting the sign of the contour (positive for anticlockwise). In general we have

$$E(\omega) = -2\pi i\{\mathrm{Res}[e^{i\omega t}E(t), t_1] + \mathrm{Res}[e^{i\omega t}E(t), t_2]\}, \tag{A17}$$

and from (A9) the following cases arise.

(i) ($\omega > 0$):

$$E(\omega) = 0, \tag{A18}$$

$$E^*(-\omega) = (-2\pi i\{\mathrm{Res}[e^{-i\omega t}E(t), t_1] + \mathrm{Res}[e^{-i\omega t}E(t), t_2]\})^*. \tag{A19}$$

(ii) ($\omega < 0$):

$$E(\omega) = -2\pi i\{\mathrm{Res}[e^{i\omega t}E(t), t_1] + \mathrm{Res}[e^{i\omega t}E(t), t_2]\}, \tag{A20}$$

$$E^*(-\omega) = 0. \tag{A21}$$

There are no poles in the upper half-plane, but reversal of the sign of ω is equivalent to integrating over the path of the lower half-plane. It is advisable to calculate the residues for higher-order poles (triple in our case) using a computer algebra system (like *Mathematica*) in order to avoid mistakes in the trivial but error-prone procedure of computing the derivatives. Finally, the residues are

$$\mathrm{Res}[e^{i\omega t}E(t), t_1] = -\frac{e^{\frac{\omega}{2}(1+q_2+i\sqrt{A})}\omega\rho(2i+\omega\sqrt{A})}{2A^{3/2}}, \tag{A22}$$

$$\mathrm{Res}[e^{i\omega t}E(t), t_2] = -\frac{e^{\frac{\omega}{2}(1+q_2-i\sqrt{A})}\omega\rho(-2i+\omega\sqrt{A})}{2A^{3/2}}, \tag{A23}$$

$$\mathrm{Res}[e^{-i\omega t}E(t), t_1] = -\frac{e^{-\frac{\omega}{2}(1+q_2+i\sqrt{A})}\omega\rho(-2i+\omega\sqrt{A})}{2A^{3/2}}, \tag{A24}$$

$$\mathrm{Res}[e^{-i\omega t}E(t), t_2] = -\frac{e^{-\frac{\omega}{2}(1+q_2-i\sqrt{A})}\omega\rho(2i+\omega\sqrt{A})}{2A^{3/2}}. \tag{A25}$$

For $\omega = 0$, the choice of the contour does not alter the result and knowing that there are no poles in the upper half-plane and the line of real values, the calculus of residues gives immediately the answer of having a zero integral. That is, there are no dc components in the field.

Finally, the Fourier transform for the TE 1-cycle pulse is given by the equation

$$E_{\mathrm{re}}(\omega) = \begin{cases} \left[i\pi\omega\rho e^{-\frac{\omega(q_2+1)}{2}} \frac{e^{\frac{i\omega}{2}\sqrt{A}}(2i+\omega\sqrt{A}) + e^{-\frac{i\omega}{2}\sqrt{A}}(-2i+\omega\sqrt{A})}{2A^{3/2}}\right]^*, & \omega > 0 \\ i\pi\omega\rho e^{\frac{\omega(q_2+1)}{2}} \frac{e^{-\frac{\omega i}{2}\sqrt{A}}(-2i+\omega\sqrt{A}) + e^{\frac{\omega i}{2}\sqrt{A}}(2i+\omega\sqrt{A})}{2A^{3/2}}, & \omega < 0 \\ 0, & \omega = 0 \end{cases} \tag{A26}$$

with

$$A \equiv A(\rho, z, q_2) = -(-1+q_2-2\rho-2iz)(-1+q_2+2\rho-2iz), \tag{A27}$$

which can be simplified to a single line, given that for the Fourier transform of a real function, it holds that $F(\omega) = F^*(-\omega)$.

It is now clear from Eqs. (A6)–(A8) that the magnetic fields satisfy the necessary conditions to apply Jordan's lemma and that they have the same poles with the electric field. Hence, the exact same approach can be used, leading to the following frequency domain expressions for the magnetic field:

$$H_{\rho,\mathrm{re}}(\omega) = \begin{cases} \left[(q_2 - 1 - 2iz)\pi\rho e^{\frac{-\omega(q_2+1)}{2}}\left(-\frac{e^{\frac{\omega i}{2}\sqrt{A}}\left(-12+6i\sqrt{A}\omega+A\omega^2\right)}{2A^{5/2}} + \frac{e^{\frac{-\omega i}{2}\sqrt{A}}\left(-12-6i\sqrt{A}\omega+A\omega^2\right)}{2A^{5/2}}\right)\right]^*, & \omega > 0 \\ (q_2 - 1 - 2iz)\pi\rho e^{\frac{\omega(q_2+1)}{2}}\left(-\frac{e^{-\frac{\omega i}{2}\sqrt{A}}\left(-12-6i\sqrt{A}\omega+A\omega^2\right)}{2A^{5/2}} + \frac{e^{\frac{\omega i}{2}\sqrt{A}}\left(-12+6i\sqrt{A}\omega+A\omega^2\right)}{2A^{5/2}}\right), & \omega < 0 \\ 0, & \omega = 0 \end{cases} \tag{A28}$$

$$H_{z,\mathrm{re}}(\omega) = \begin{cases} \left[-\pi i e^{\frac{-\omega(q_2+1)}{2}}\left(\frac{e^{\frac{\omega i}{2}\sqrt{A}}\left[Ar^2\omega^2+(A-6r^2)(2-i\sqrt{A}\omega)\right]}{A^{5/2}} + \frac{e^{-\frac{\omega i}{2}\sqrt{A}}\left[-Ar^2\omega^2+(A-6r^2)(-2-i\sqrt{A}\omega)\right]}{A^{5/2}}\right)\right]^*, & \omega > 0 \\ -\pi i e^{\frac{\omega(q_2+1)}{2}}\left(\frac{e^{-\frac{\omega i}{2}\sqrt{A}}\left[Ar^2\omega^2+(A-6r^2)(2+i\sqrt{A}\omega)\right]}{A^{5/2}} + \frac{e^{\frac{\omega i}{2}\sqrt{A}}\left[-Ar^2\omega^2+(A-6r^2)(-2+i\sqrt{A}\omega)\right]}{A^{5/2}}\right), & \omega < 0 \\ 0, & \omega = 0. \end{cases} \tag{A29}$$

Of course, one has to return to dimensional variables and insert the omitted coefficient in order to have the actual fields as follows:

$$E_{\mathrm{re}}(\omega) = \begin{cases} 4f_0\sqrt{\mu_0/\epsilon_0}\left[i\pi\frac{\omega}{c^2}\frac{\rho}{q_1}e^{-\frac{\omega(q_2+q_1)}{2c}}\frac{e^{\frac{i\omega}{2c}\sqrt{A}}\left(2ci+\omega\sqrt{A}\right)+e^{-\frac{i\omega}{2c}\sqrt{A}}\left(-2ci+\omega\sqrt{A}\right)}{2A^{3/2}}\right]^*, & \omega > 0 \\ 4f_0\sqrt{\mu_0/\epsilon_0}i\pi\frac{\omega}{c^2}\frac{\rho}{q_1}e^{\frac{\omega(q_2+q_1)}{2c}}\frac{e^{-\frac{\omega i}{2c}\sqrt{A}}\left(-2ci+\omega\sqrt{A}\right)+e^{\frac{\omega i}{2c}\sqrt{A}}\left(2ci+\omega\sqrt{A}\right)}{2A^{3/2}}, & \omega < 0 \\ 0, & \omega = 0 \end{cases} \tag{A30}$$

$$H_{\rho,\mathrm{re}}(\omega) = \begin{cases} \left[4f_0\pi\rho\frac{(q_2-q_1-2iz)}{q_1c^2}e^{\frac{-\omega(q_2+q_1)}{2c}}\left(-\frac{e^{\frac{\omega i}{2c}\sqrt{A}}\left(-12c^2+6i\sqrt{A}\omega c+A\omega^2\right)}{2A^{5/2}} + \frac{e^{\frac{-\omega i}{2c}\sqrt{A}}\left(-12c^2-6i\sqrt{A}\omega c+A\omega^2\right)}{2A^{5/2}}\right)\right]^*, & \omega > 0 \\ 4f_0\pi\rho\frac{(q_2-q_1-2iz)}{q_1c^2}e^{\frac{\omega(q_2+q_1)}{2c}}\left(-\frac{e^{-\frac{\omega i}{2c}\sqrt{A}}\left(-12c^2-6i\sqrt{A}\omega c+A\omega^2\right)}{2A^{5/2}} + \frac{e^{\frac{\omega i}{2c}\sqrt{A}}\left(-12c^2+6i\sqrt{A}\omega c+A\omega^2\right)}{2A^{5/2}}\right), & \omega < 0 \\ 0, & \omega = 0 \end{cases} \tag{A31}$$

$$H_{z,\mathrm{re}}(\omega) = \begin{cases} \left[-\frac{4\pi i f_0}{q_1 c}e^{\frac{-\omega(q_2+q_1)}{2c}}\left(\frac{e^{\frac{\omega i}{2c}\sqrt{A}}\left[Ar^2\omega^2/c+(A-6r^2)(2c-i\sqrt{A}\omega)\right]}{A^{5/2}} + \frac{e^{\frac{-\omega i}{2c}\sqrt{A}}\left[-Ar^2\omega^2/c+(A-6r^2)(-2c-i\sqrt{A}\omega)\right]}{A^{5/2}}\right)\right]^*, & \omega > 0 \\ -\frac{4\pi i f_0}{q_1 c}e^{\frac{\omega(q_2+q_1)}{2c}}\left(\frac{e^{-\frac{\omega i}{2c}\sqrt{A}}\left[Ar^2\omega^2/c+(A-6r^2)(2c+i\sqrt{A}\omega)\right]}{A^{5/2}} + \frac{e^{\frac{\omega i}{2c}\sqrt{A}}\left[-Ar^2\omega^2/c+(A-6r^2)(-2c+i\sqrt{A}\omega)\right]}{A^{5/2}}\right), & \omega < 0 \\ 0, & \omega = 0 \end{cases} \tag{A32}$$

with

$$A \equiv A(\rho, z, q_2) = -(-q_1 + q_2 - 2\rho - 2iz)(-q_1 + q_2 + 2\rho - 2iz). \tag{A33}$$

Because now of the analyticity of Eqs. (A3)–(A5), with respect to time, the real and imaginary parts (or, equivalently, the 1-cycle and $1\frac{1}{2}$-cycle) form Hilbert transform pairs, which means that they share the same spectrum with a change only in phase, as it is clear from the following relations [12,26]:

$$\mathbf{E}_{\mathrm{im}}(\omega) = i\,\mathrm{sgn}(\omega)\mathbf{E}_{\mathrm{re}}(\omega) \tag{A34}$$

and

$$\mathbf{H}_{\mathrm{im}}(\omega) = i\,\mathrm{sgn}(\omega)\mathbf{H}_{\mathrm{re}}(\omega), \tag{A35}$$

with

$$\mathrm{sgn}(\omega) = \begin{cases} 1, & \omega > 0 \\ -1, & \omega < 0 \\ 0, & \omega = 0. \end{cases} \tag{A36}$$

Finally, regarding the TM pulses, the frequency domain equations can be derived by a substitution of the TE formulas to the following equations:

$$\mathbf{E}_{\mathrm{TM}} = \sqrt{\frac{\mu_0}{\epsilon_0}}\mathbf{H}_{\mathrm{TE}}, \tag{A37}$$

$$\mathbf{H}_{\mathrm{TM}} = -\sqrt{\frac{\epsilon_0}{\mu_0}}\mathbf{E}_{\mathrm{TE}}. \tag{A38}$$

APPENDIX B: PROOF OF ISODIFFRACTION FOR WELL-COLLIMATED DONUT PULSES

We now prove that in the paraxial regime of well-collimated pulses $q_2 \gg q_1$, the FD pulse is isodiffracting. We show that, far from the focus, in each cross section of the beam perpendicular to the direction of propagation the spatial profiles of intensity for every frequency component of the beam scale along the trajectory of the beam in the same way. This is achieved by tracing the radial position of the maxima of each spectral component $\rho_{\max}(\omega)$ and showing that the ratio of these radial positions between any two monochromatic beams is independent of the propagation distance z, $\rho_{\max}(\omega_2)/\rho_{\max}(\omega_1) = \mathrm{const}$, and that smaller wavelengths are always closer to the center of the beam. We finally derive

an approximate expression for the divergence angle of each spectral component where we show that it is proportional to the square root of its wavelength. A comparison with the divergence angle of Gaussian beams shows that such dependence corresponds to isodiffracting beams and thus all spectral components of the FD share the same Rayleigh length that it is shown to be proportional to q_2.

Since the spectrum is symmetric with respect to the $z = 0$ plane, which is the focal plane, we can prove the isodiffracting property of the pulse for $z > 0$ without loss of generality. The same is true for ω and hence we restrict our analysis to $z > 0$ and $\omega > 0$. It turns out that in this case the Fourier transform of the pulse is simplified to the following equation:

$$E^*_{\mathrm{re}}(\omega) = i\pi\omega\rho e^{-\frac{\omega(q_2+1)}{2}} \frac{e^{-\frac{i\omega}{2}\sqrt{A}}(-2i+\omega\sqrt{A})}{2A^{3/2}}. \tag{B1}$$

That is because $\mathrm{Im}(\sqrt{A}) > 0$ and hence the positive exponential of Eq. (A30):

$$e^{\frac{i\omega}{2}\sqrt{A}} = e^{\frac{i\omega}{2}\mathrm{Re}(\sqrt{A})} e^{\frac{-\omega}{2}\mathrm{Im}(\sqrt{A})} \tag{B2}$$

is negligible compared to the negative exponential

$$e^{\frac{-i\omega}{2}\sqrt{A}} = e^{-\frac{i\omega}{2}\mathrm{Re}(\sqrt{A})} e^{\frac{\omega}{2}\mathrm{Im}(\sqrt{A})} \tag{B3}$$

and thus it can be ignored. The spectrum of the electric field is now given by the following equation:

$$\begin{aligned} I_{\mathrm{re}}(\omega) &= E_{\mathrm{re}}(\omega)E^*_{\mathrm{re}}(\omega) \\ &= \pi^2\omega^2\rho^2 e^{-\omega(q_2+1)} \frac{e^{\omega\,\mathrm{Im}(\sqrt{A})}[4 - 4\omega\,\mathrm{Im}(\sqrt{A}) + \omega|A|]}{2|A|^3}. \end{aligned} \tag{B4}$$

For $z \gg q_2$ we can write

$$|A| = 4(z^2 + \rho^2) \tag{B5}$$

and

$$\begin{aligned} \mathrm{Im}(\sqrt{A}) &= \sqrt{|A|}\sin\left[\frac{1}{2}\mathrm{Arg}(A)\right] \\ &= \sqrt{|A|}\sin\left[\frac{1}{2}\arctan\left(\frac{4(q_2-1)z}{4z^2 + 4\rho^2 - (q_2-1)^2}\right)\right] \\ &= \frac{(q_2-1)z}{\sqrt{z^2+\rho^2}} \end{aligned} \tag{B6}$$

since $\sin(x) \simeq x$ and $\arctan(x) \simeq x$ for $x \ll 1$. In addition, $|A| \gg \mathrm{Im}(\sqrt{A})$ and $|A| \gg 4$ leading to a simplified expression for the spectrum in the far field

$$I_{\mathrm{re}}(\omega) = \pi^2\omega^3\rho^2 e^{-\omega(q_2+1)} \frac{e^{\frac{\omega(q_2-1)z}{\sqrt{z^2+\rho^2}}}}{32(z^2+\rho^2)^2}. \tag{B7}$$

The general shape of the spectrum is the same for any frequency and propagation distance since it is given by the same equation. This equation has only one extrema which is the maximum of the intensity. That is easy to see since the function is actually the product of a decreasing exponential with the ratio of a second-degree parabola and a shifted fourth-degree parabola. The ratio has only one maximum and the exponential is simply shifting this maximum in space. Hence, we only have to find the position of this maximum. That is the zero of the derivative of the intensity with respect to the radius $\frac{dI_{\mathrm{re}}(\omega,\rho)}{d\rho}|_{\rho_{\max}} = 0$, which is given by the solution of the following equation:

$$4x^3 - [4 + \omega^2(q_2-1)^2]z^2x^2 - 4z^4x + 4z^6 = 0 \tag{B8}$$

with $\rho_{\max} = \sqrt{x_0}$, where x_0 is the only real solution of Eq. (B8). However, in the paraxial case, the radial expansion of the beam increases with a much smaller rate than the propagation distance z. Hence, the first term of the polynomial $x^3 = \rho^6$ will be very small compared to the rest terms containing z and thus it can be ignored. Finally, the equation to be solved becomes

$$[4 + \omega^2(q_2-1)^2]x^2 + 4z^2x - 4z^4 = 0 \tag{B9}$$

and the radial position of the maximum electric field amplitude for each spectral component in the far field is given by the following simple equation:

$$\rho_{\max} = z\sqrt{\frac{-2 + 2\sqrt{5 + (q_2-1)^2\omega^2}}{4 + (q_2-1)^2\omega^2}}. \tag{B10}$$

The ratio of the radial position of the maxima between two different wavelengths is easily obtained as

$$\begin{aligned} \xi(\omega_2) &= \frac{\rho_{\max}(\omega_2)}{\rho_{\max}(\omega_1)} \\ &= \sqrt{\frac{[4 + (q_2-1)^2\omega_1^2]\left[-2 + 2\sqrt{5 + (q_2-1)^2\omega_2^2}\right]}{\left[-2 + 2\sqrt{5 + (q_2-1)^2\omega_1^2}\right][4 + (q_2-1)^2\omega_2^2]}} \end{aligned} \tag{B11}$$

and is independent of the propagation distance z. In addition, it is easy to prove that Eq. (B10) is a monotonically decreasing function of ω.

To illustrate the validity of Eq. (B11), we plot the radial position of the maximum intensity of the FD pulse for each wavelength and increasing propagation distance z/q_1 with $q_2 = 100q_1$ [see Fig. 6(a)]. Then, we use as a reference frequency the smallest frequency on the plot $\omega_1 q_1/2\pi c = 0.1$ and calculate the ratio of the position of the maxima for all frequencies up to $\omega q_1/2\pi c = 0.8$, $\frac{\rho_{\max}(\omega)}{\rho_{\max}(\omega_1)}$. We do this for various values of propagation distance z/q_1 [Fig. 6(b)] and parameter q_2 [Fig. 6(c)]. For $z \gg q_2$ and $q_2 \gg q_1$ the value of the ratio is similar to the theoretically predicted value from Eq. (B11) verifying its validity. Additionally, we note that the ratio is always smaller than unity, which indicates that the shorter wavelengths exhibit peak values of spectral intensity at smaller radii in accordance with Fig. 2(c) of the main text. As predicted by Eq. (B11), away from focus the ratio is independent of the propagation distance [see Fig. 6(b)]. From Fig. 6(b) we also notice that the ratio ξ varies very little even at focus which is an indication that the FD pulse is isodiffracting. From Fig. 6(c) and for $q_2 \gg q_1$ we notice that the ratio becomes independent of the parameter q_2, meaning that for very well-collimated beams the ratio of the position of the maxima between two frequencies can be described by a

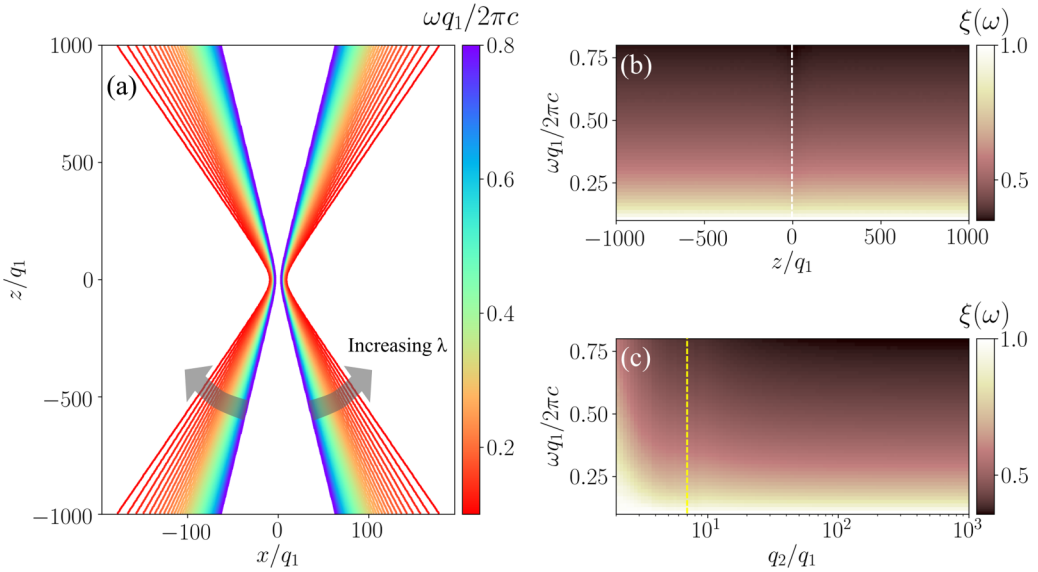

FIG. 6. (a) Trace of the position of the maximum intensity for each wavelength. (b) Numerical calculation of the dimensionless ratio of the radial position of the maxima between a reference frequency $\omega_1 q_1/2\pi c = 0.1$ and a variable frequency ω, for $q_2 = 100q_1$ and for increasing propagation distance z/q_1. The white dashed line indicates the position of the focus. (c) Numerical calculation of the same ratio for fixed distance $z/q_1 = 1000$ and for increasing q_2. For $z \gg q_2$ and $q_2 \gg q_1$ the value of the ratio is similar to the theoretically predicted value from Eq. (B11). The yellow dashed line indicates the limit of q_2/q_1 below which Eq. (B11) deviates from the actual value.

very simple expression that is proportional to the ratio of the frequencies.

Finally, Eq. (B10) is true for $z \gg q_1$ and thus is appropriate for the calculation of the divergence angle of each beam. Since all our calculations are for the paraxial regime $q_2 \gg q_1$, the angle of divergence is small and can be given approximately as

$$\Theta_{\text{div}} \simeq \arctan\left(\frac{\rho_{\max}}{z}\right) \simeq \sqrt{\frac{-2+2\sqrt{5+(q_2-1)^2\omega^2}}{4+(q_2-1)^2\omega^2}} \simeq \sqrt{\frac{2}{q_2\omega}}. \tag{B12}$$

The important thing to notice here is the similarity with the expression of the divergence angle of a Gaussian beam $\Theta_{\text{div}} \simeq \sqrt{\lambda/z_R\pi}$, where z_R is the Rayleigh length [27]. It is now clear that the parameter q_2 has the role of the Rayleigh length and since it does not depend on the wavelength the beams that compose the FD pulse are isodiffracting.

APPENDIX C: HANKEL TRANSFORM

By using Jordan's lemma in a similar way with Appendix A, an analytical expression for one of the spatial coordinates of the FD pulse can be derived. However, it is clear that the pulse does not depend on the polar angle θ. This symmetry can be exploited and a Hankel transform can be applied for the calculation of the spatial frequencies in a transverse plane r, θ [18]. In our case, the intensity of the pulse is circularly invariant but the field is not. It has a polarization singularity at the center leading to a sign inversion of the field across a line passing through the center of the pulse.

In this Appendix we derive a closed-form expression for the Hankel transform of the electric field of the TE pulse. A similar analysis can be applied for the TM pulse. In order to deal with the polarization we start by projecting the $\hat{\boldsymbol{\theta}}$ dependence of the field to the $\hat{\boldsymbol{x}}$, $\hat{\boldsymbol{y}}$ plane. The following relations between Cartesian and polar coordinates will be used:

$$\begin{aligned} \rho &= \sqrt{x^2+y^2}, & \hat{\boldsymbol{\rho}} &= \cos\theta\hat{\boldsymbol{x}} + \sin\theta\hat{\boldsymbol{y}}, \\ \theta &= \arctan\left(\frac{y}{x}\right), & \hat{\boldsymbol{\theta}} &= -\sin\theta\hat{\boldsymbol{x}} + \cos\theta\hat{\boldsymbol{y}}, \\ x &= \rho\cos\theta, & \hat{\boldsymbol{x}} &= \cos\theta\hat{\boldsymbol{\rho}} - \sin\theta\hat{\boldsymbol{\theta}}, \\ y &= \rho\sin\theta, & \hat{\boldsymbol{y}} &= \sin\theta\hat{\boldsymbol{\rho}} + \cos\theta\hat{\boldsymbol{\theta}} \end{aligned} \tag{C1}$$

for the real space and

$$\begin{aligned} k_\rho &= \sqrt{k_x^2+k_y^2}, & \hat{\boldsymbol{k}}_{\boldsymbol{\rho}} &= \cos k_\theta\hat{\boldsymbol{k}}_{\boldsymbol{x}} + \sin k_\theta\hat{\boldsymbol{k}}_{\boldsymbol{y}}, \\ k_\theta &= \arctan\left(\frac{k_y}{k_x}\right), & \hat{\boldsymbol{k}}_{\boldsymbol{\theta}} &= -\sin k_\theta\hat{\boldsymbol{k}}_{\boldsymbol{x}} + \cos k_\theta\hat{\boldsymbol{k}}_{\boldsymbol{y}}, \\ k_x &= k_\rho\cos k_\theta, & \hat{\boldsymbol{k}}_{\boldsymbol{x}} &= \cos k_\theta\hat{\boldsymbol{k}}_{\boldsymbol{\rho}} - \sin k_\theta\hat{\boldsymbol{k}}_{\boldsymbol{\phi}}, \\ k_y &= k_\rho\sin k_\theta, & \hat{\boldsymbol{k}}_{\boldsymbol{y}} &= \sin k_\theta\hat{\boldsymbol{k}}_{\boldsymbol{\rho}} + \cos k_\theta\hat{\boldsymbol{k}}_{\boldsymbol{\phi}} \end{aligned} \tag{C2}$$

for the k space. From the above we have

$$\mathbf{E}(\rho,\theta) = -\sin\theta E_\theta(\rho)\hat{\boldsymbol{x}} + \cos\theta E_\theta(\rho)\hat{\boldsymbol{y}}. \tag{C3}$$

It is now clear that each polarization of the field is separable in the polar coordinates. In that case, the Fourier transform can be expressed as an infinite sum of weighted Hankel transforms [18]. Let $\mathcal{F}$ and $\mathcal{H}$ denote the Fourier and Hankel transforms of a function, respectively, and $g(\rho,\theta) = g_\theta(\theta)g_\rho(\rho)$ being the separable function to be Fourier transformed. Then, we can write

$$\mathcal{F}[g(\rho,\theta)] = \sum_{-\infty}^{\infty} c_m(-i)^m e^{imk_\theta}\mathcal{H}_m[g_\rho(\rho)], \tag{C4}$$

with

$$c_m = \frac{1}{2\pi}\int_0^{\infty} g_\theta(\theta)e^{-im\theta}d\theta, \tag{C5}$$

$$\mathcal{H}[g_\rho(\rho)] = 2\pi\int_0^{\infty}\rho g_\rho(\rho)J_m(k_\rho\rho)d\rho \tag{C6}$$

and J_m the m-order Bessel function of the first kind. If the azimuthal part of the field $g_\theta(\theta)$ has some kind of azimuthal symmetry, as in our case, then only a few terms of the infinite sum will contribute to the result making the problem tractable.

For the E_x component we have $g_\theta(\theta) = -\sin\theta$ and

$$\begin{aligned} c_m &= \frac{-1}{2\pi}\int_0^{2\pi}\sin\theta e^{-im\theta}d\theta \\ &= \frac{-1}{2\pi}\int_0^{2\pi}\frac{e^{-i\theta(m-1)}}{2i}d\theta + \frac{1}{2\pi}\int_0^{2\pi}\frac{e^{-i\theta(m+1)}}{2i}d\theta \\ &= \begin{cases} -\frac{1}{2i}, & m = 1 \\ \frac{1}{2i}, & m = -1 \\ 0, & m \neq \pm 1 \end{cases} \end{aligned} \tag{C7}$$

and for the E_y, $g_\theta(\theta) = \cos\theta$ and

$$c_m = \begin{cases} \frac{1}{2}, & m \pm 1 \\ 0, & m \neq \pm 1. \end{cases} \tag{C8}$$

Hence, from Eqs. (C3)–(C8) and by using the identity $J_{-n}(x) = (-1)^n J_n(x)$ we have

$$E_x(k_\rho, k_\theta)\hat{\boldsymbol{x}} = 2\pi i\,\sin k_\theta\int_0^{\infty}\rho E_\theta(\rho)J_1(k_\rho\rho)d\rho\,\hat{\boldsymbol{x}} \tag{C9}$$

and

$$E_y(k_\rho, k_\theta)\hat{\boldsymbol{y}} = -2\pi i\,\cos k_\theta\int_0^{\infty}\rho E_\theta(\rho)J_1(k_\rho\rho)d\rho\,\hat{\boldsymbol{y}}. \tag{C10}$$

However, since $\hat{\boldsymbol{x}}, \hat{\boldsymbol{y}}, \hat{\boldsymbol{\theta}}, \hat{\boldsymbol{k}}_{\boldsymbol{x}}, \hat{\boldsymbol{k}}_{\boldsymbol{y}}$, and $\hat{\boldsymbol{k}}_{\boldsymbol{\theta}}$ are unit vectors in the same coordinate system, $\hat{\boldsymbol{x}} = \hat{\boldsymbol{k}}_{\boldsymbol{x}}$, $\hat{\boldsymbol{y}} = \hat{\boldsymbol{k}}_{\boldsymbol{y}}$, and $\hat{\boldsymbol{\theta}} = \hat{\boldsymbol{k}}_{\boldsymbol{\theta}}$ leading to a single azimuthally polarized equation without a k_θ dependence

$$\mathbf{E}(k_\rho) = -2\pi i\int_0^{\infty}\rho E_\theta(\rho)J_1(k_\rho\rho)d\rho\,\hat{\boldsymbol{\theta}}. \tag{C11}$$

For the inverse transform we have to look first at the definition of the forward transform that was used to derive Eq. (C11):

$$\begin{aligned} \mathbf{E}(k_\rho, k_\theta) = &\int_0^{2\pi}\int_0^{\infty} -\sin\theta e^{-ik_\rho\rho(\cos\theta\cos k_\theta+\sin\theta\sin k_\theta)}E_\theta(\rho)\rho\,d\rho\,d\theta\,\hat{\boldsymbol{x}} \\ &+\int_0^{2\pi}\int_0^{\infty}\cos\theta e^{-ik_\rho\rho(\cos\theta\cos k_\theta+\sin\theta\sin k_\theta)}E_\theta(\rho)\rho\,d\rho\,d\theta\,\hat{\boldsymbol{y}}. \end{aligned} \tag{C12}$$

In the same manner we can write the inverse as

$$\begin{aligned} \mathbf{E}(\rho,\theta) = &\frac{1}{4\pi^2}\int_0^{2\pi}\int_0^{\infty} -\sin k_\theta e^{ik_\rho\rho(\cos\theta\cos k_\theta+\sin\theta\sin k_\theta)}E_\theta(k_\rho)k_\rho dk_\rho dk_\theta\hat{\boldsymbol{k}}_{\boldsymbol{x}} \\ &+\frac{1}{4\pi^2}\int_0^{2\pi}\int_0^{\infty}\cos k_\theta e^{ik_\rho\rho(\cos\theta\cos k_\theta+\sin\theta\sin k_\theta)}E_\theta(k_\rho)k_\rho dk_\rho dk_\theta\hat{\boldsymbol{k}}_{\boldsymbol{y}}. \end{aligned} \tag{C13}$$

Finally, we define $\theta' = \theta - \pi$, hence, $\sin(\theta'+\pi) = -\sin\theta'$ and $\cos(\theta'+\pi) = -\cos\theta'$. The integral limits change to $(-\pi, \pi)$ but since the integrand has a period of 2π this does not change the integral and hence there is no need to change the limits. By ignoring the prime at θ' for clarity we end up with the following equation for the inverse Fourier transform:

$$\begin{aligned} \mathbf{E}(\rho,\theta) = &\frac{1}{4\pi^2}\int_0^{2\pi}\int_0^{\infty}\sin k_\theta e^{-ik_\rho\rho(\cos\theta\cos k_\theta+\sin\theta\sin k_\theta)}E_\theta(k_\rho)k_\rho dk_\rho dk_\theta\hat{\boldsymbol{k}}_{\boldsymbol{x}} \\ &+\frac{1}{4\pi^2}\int_0^{2\pi}\int_0^{\infty} -\cos k_\theta e^{-ik_\rho\rho(\cos\theta\cos k_\theta+\sin\theta\sin k_\theta)}E_\theta(k_\rho)k_\rho dk_\rho dk_\theta\hat{\boldsymbol{k}}_{\boldsymbol{y}}. \end{aligned} \tag{C14}$$

It is now clear that by swapping ρ with k_ρ and θ with k_θ, Eq. (C14) is identical to Eq. (C12) with the exception of the coefficient $\frac{1}{4\pi^2}$ and a minus sign. Hence, the inverse Fourier transform can be given from the following Hankel transform:

$$\mathbf{E}(\rho) = \frac{i}{2\pi}\int_0^{\infty}k_\rho E_\theta(k_\rho)J_1(k_\rho\rho)dk_\rho\hat{\boldsymbol{\theta}}. \tag{C15}$$

Returning to Eq. (C11), we will solve the integral for the complex expression of the field. The transforms of the real and imaginary fields are then simply taken from the following equations:

$$E_{\mathrm{re},\theta}(k_\rho) = \frac{E_\theta(k_\rho) - E_\theta^*(k_\rho)}{2}, \tag{C16}$$

$$E_{\mathrm{im},\theta}(k_\rho) = \frac{E_\theta(k_\rho) + E_\theta^*(k_\rho)}{2i}. \tag{C17}$$

Proof.

$$\begin{aligned} E_{\mathrm{re},\theta}(k_\rho) &= -2\pi i \int_0^\infty \mathrm{Re}[E_\theta(\rho)] J_1(k_\rho\rho)\rho\, d\rho \\ &= \int_0^\infty \frac{-2\pi i E_\theta(\rho)}{2} J_1(k_\rho\rho)\rho\, d\rho \\ &\quad - \left[\int_0^\infty \frac{-2\pi i E_\theta(\rho)}{2} J_1(k_\rho\rho)\rho\, d\rho\right]^* \\ &= \frac{E_\theta(k_\rho) - E_\theta^*(k_\rho)}{2} \end{aligned}$$

and similar for the imaginary part, given that k_ρ and ρ are real. ■

For clarity, we rewrite the electric field expression as

$$\begin{aligned} E_\theta &= -4if_0\sqrt{\frac{\mu_0}{\epsilon_0}} \frac{\rho(q_1+q_2-2ict)}{[\rho^2+(q_1+iz-ict)(q_2-iz-ict)]^3} \\ &= \mathrm{coef}\frac{\rho}{(\rho^2+\alpha^2)^3} \end{aligned} \tag{C18}$$

with $\mathrm{coef} = -4if_0\sqrt{\frac{\mu_0}{\epsilon_0}}(q_1+q_2-2ict)$ and $\alpha = \sqrt{(q_1+iz-ict)(q_2-iz-ict)}$. The integral that we have to solve now becomes

$$E_\theta(k_\rho) = -2\pi i\,\mathrm{coef}\int_0^\infty \frac{\rho^2}{(\rho^2+\alpha^2)^3} J_1(k_\rho\rho) d\rho. \tag{C19}$$

The solution of an integral of the above form is known when it satisfies some criteria and it is given from the form [28,29]

$$\int_0^\infty \frac{\rho^{\nu+1}}{(\rho^2+\alpha^2)^{\mu+1}} J_\nu(k\rho) d\rho = \frac{k^\mu \alpha^{\nu-\mu}}{2^\mu \Gamma(\mu+1)} K_{\nu-\mu}(k\alpha) \tag{C20}$$

with $\mathrm{Re}(\alpha) > 0$ and $-1 < \mathrm{Re}(\nu) < 2\,\mathrm{Re}(\mu) + 3/2$. K_ν is the ν-order modified Bessel function of the second kind and Γ denotes the gamma function with its integral definition being [25]

$$\Gamma(z) = \int_0^\infty t^{z-1} e^t dt,\ \mathrm{Re}(z) > 0. \tag{C21}$$

The only properties of this function that we will need here are

$$\Gamma(z+1) = z\Gamma(z), \tag{C22}$$

$$\Gamma(1) = 1. \tag{C23}$$

In our case, $\nu = 1$ and $\mu = 2$ and hence the second criterion is satisfied. The first criterion requires $\mathrm{Re}(\alpha) > 0$ or $|\arg(\alpha)| < \pi/2$. We will now show that $|\arg(\alpha)| < \pi/2$ is true in our case and hence all the conditions needed to apply the above formula are met.

Proof. We have

$$\alpha = \sqrt{q_1q_2 + z^2 - c^2t^2 - i[ct(q_1+q_2) + z(q_1-q_2)]},$$

$$\beta = \alpha^2 = q_1q_2 + z^2 - c^2t^2 - i[ct(q_1+q_2) + z(q_1-q_2)].$$

We want to study when $|\arg(\alpha)| < \pi/2$ or, since $\alpha = \sqrt{\beta} = \sqrt{|\beta|e^{i\theta}} = \sqrt{|\beta|}e^{i\theta/2}$, when $|\arg(\beta)| = |\arg(\alpha^2)| < \pi$. We write $\beta = x + yi$ and, hence, $\arg(\beta) = \mathrm{atan2}(y, x)$. From Eq. (A15) there is only one case that the criterion can be possibly violated, the case $\arctan(y/x) + \pi$ with $x < 0,\ y \geqslant 0$. But $-\pi/2 < \arctan(y/x) \leqslant 0$ and, hence, the equality $|\arg(\alpha)| = \pi/2$ can only happen when $y = 0$ and $x < 0$.

For $y = 0$ we have

$$ct = \frac{q_2 - q_1}{q_2 + q_1} z. \tag{C24}$$

For $x < 0$ we have

$$c^2t^2 > q_1q_2 + z^2. \tag{C25}$$

Substitution of Eqs. (C24) to (C25) leads to the following statement:

$$\frac{-4q_1q_2}{(q_1+q_2)^2} z^2 > q_1q_2 \tag{C26}$$

which is not true since q_1 and q_2 are both positive numbers. Hence, $|\arg(\alpha)|$ is always smaller than $\pi/2$. ■

The Hankel transform is now given by the equation

$$E_\theta(k_\rho) = -2\pi i\,\mathrm{coef}\frac{k_\rho^2}{8\alpha} K_{-1}(k_\rho\alpha). \tag{C27}$$

From the definition of the K_ν it can be easily shown that $K_{-1}(x) = K_1(x)$, hence, we finally have

$$\mathbf{E}(k_\rho) = -\pi f_0\sqrt{\frac{\mu_0}{\epsilon_0}}(q_1+q_2-2ict)\frac{k_\rho^2}{\alpha} K_1(k_\rho\alpha)\hat{\boldsymbol{\theta}}, \tag{C28}$$

with $\alpha = \sqrt{(q_1+iz-ict)(q_2-iz-ict)}$.

Finally, an alternative route for this derivation can be followed by starting from the definition of the scalar function f [Eq. (3)]. This function can be written as a superposition of bidirectional waves [21] that are solutions of the scalar wave equation and their integral representation directly leads to an integral for the Hankel transform of the fields.

[1] R. W. Hellwarth and P. Nouchi, Focused one-cycle electromagnetic pulses, Phys. Rev. E **54**, 889 (1996).

[2] A. Zdagkas, N. Papasimakis, V. Savinov, M. R. Dennis, and N. I. Zheludev, Singularities in the flying electromagnetic doughnuts, Nanophotonics **8**, 1379 (2019).

[3] T. Raybould, V. Fedotov, N. Papasimakis, I. Youngs, and N. Zheludev, Focused electromagnetic doughnut pulses and their interaction with interfaces and nanostructures, Opt. Express **24**, 3150 (2016).

[4] T. Kaelberer, V. A. Fedotov, N. Papasimakis, D. P. Tsai, and N. I. Zheludev, Toroidal dipolar response in a metamaterial, Science **330**, 1510 (2010).

[5] N. Papasimakis, V. A. Fedotov, V. Savinov, T. A. Raybould, and N. I. Zheludev, Electromagnetic toroidal excitations in matter and free space, Nat. Mater. **15**, 263 (2016).

[6] T. Raybould, V. A. Fedotov, N. Papasimakis, I. Youngs, and N. I. Zheludev, Exciting dynamic anapoles with electromagnetic doughnut pulses, Appl. Phys. Lett. **111**, 081104 (2017).

[7] J. Neill Brittingham, Focus waves modes in homogeneous Maxwells equations: Transverse electric mode, J. Appl. Phys. **54**, 1179 (1983).

[8] T. T. Wu and R. W. P. King, Comment on "focus wave modes in homogeneous maxwell's equations: Transverse electric mode", J. Appl. Phys. **56**, 2587 (1984).

[9] R. W. Ziolkowski, Localized transmission of electromagnetic energy, Phys. Rev. A **39**, 2005 (1989).

[10] R. W. Ziolkowski, Exact solutions of the wave equation with complex source locations, J. Math. Phys. **26**, 861 (1985).

[11] S. Feng, H. G. Winful, and R. W. Hellwarth, Gouy shift and temporal reshaping of focused single-cycle electromagnetic pulses, Opt. Lett. **23**, 385 (1998).

[12] S. Feng, H. G. Winful, and R. W. Hellwarth, Spatiotemporal evolution of focused single-cycle electromagnetic pulses, Phys. Rev. E **59**, 4630 (1999).

[13] R. W. Ziolkowski, D. K. Lewis, and B. D. Cook, Evidence of Localized Wave Transmission, Phys. Rev. Lett. **62**, 147 (1989).

[14] R. W. Ziolkowski and D. K. Lewis, Verification of the localized-wave transmission effect, J. Appl. Phys. **68**, 6083 (1990).

[15] H. E. Hernández-Figueroa, M. Zamboni-Rached, and E. Recami, *Non-diffracting Waves* (Wiley, Hoboken, NJ, 2013).

[16] N. Papasimakis, T. Raybould, V. A. Fedotov, D. P. Tsai, I. Youngs, and N. I. Zheludev, Pulse generation scheme for flying electromagnetic doughnuts, Phys. Rev. B **97**, 201409(R) (2018).

[17] A. Zdagkas, N. Papasimakis, V. Nalla, H. Zhang, O. Buchnev, and N. I. Zheludev, Generation of electromagnetic doughnut pulses with a singular metamaterial converter, in *Proceedings Nanometa* (2019), paper THU4s.2.; A. Zdagkas, Y. Hou, V. Savinov, H. Zhang, O. Buchnev, N. Papasimakis, and N. I. Zheludev, "Generation of topological space-time non-separable light pulses," in *Conference on Lasers and Electro-Optics, OSA Technical Digest* (Optical Society of America, 2020), paper FW3A.4.

[18] J. W. Goodman, *Introduction to Fourier Optics*, McGraw-Hill Physical and Quantum Electronics Series (W. H. Freeman, San Francisco, 2005).

[19] J. D. Jackson, *Classical Electrodynamics*, 3rd ed. (Wiley, New York, 1999).

[20] A. W. Norfolk and E. J. Grace, Reconstruction of optical fields with the quasi-discrete hankel transform, Opt. Express **18**, 10551 (2010).

[21] I. M. Besieris, A. M. Shaarawi, and R. W. Ziolkowski, A bidirectional traveling plane wave representation of exact solutions of the scalar wave equation, J. Math. Phys. **30**, 1254 (1989).

[22] R. Donnelly and R. Ziolkowski, A method for constructing solutions of homogeneous partial differential equations: localized waves, Proc. R. Soc. London, Ser. A **437**, 673 (1992).

[23] R. Donnelly and R. W. Ziolkowski, Designing localized waves, Proc. R. Soc. London, Ser. A **440**, 541 (1993).

[24] https://doi.org/10.5258/SOTON/D1644.

[25] G. B. Arfken, H. J. Weber, and F. E. Harris, *Mathematical Methods for Physicists: A Comprehensive Guide* (Elsevier, Amsterdam, 2012).

[26] F. W. King, *Hilbert Transforms*, Encyclopedia of Mathematics and its Applications (Cambridge University Press, Cambridge, 2009), Vol. 1.

[27] B. E. A. Saleh and M. C. Teich, *Fundamentals of Photonics*, 2nd ed., Wiley Series in Pure and Applied Optics (Wiley, New York, 2007).

[28] Q.-G. Lin, Infinite integrals involving bessel functions by an improved approach of contour integration and the residue theorem, Ramanujan J. **35**, 443 (2014).

[29] G. N. Watson, *A Treatise on the Theory of Bessel Functions* (Cambridge University Press, Cambridge, 1944).